PERGAMON

International Journal of Heat and Mass Transfer 44 (2001) 2107–2120

International Journal of HEAT and MASS TRANSFER

www.elsevier.com/locate/ijhmt

Mixed convection heat transfer in the entrance region of horizontal annuli

Nazrul Islam [a], U.N. Gaitonde [b], G.K. Sharma [b,*]

[a] *Department of Mechanical Engineering, Z.H. College of Engineering and Technology, Aligarh Muslim University, Aligarh-202 002, India*

[b] *Department of Mechanical Engineering, Indian Institute of Technology, Bombay, Powai, Mumbai-400 076, India*

Received 1 November 1996; accepted 16 June 2000

Abstract

The present study deals with a numerical investigation of steady laminar mixed convection heat transfer in a horizontal concentric annulus using air and water as the working fluid. Special attention has been paid to the entrance region effect. The thermal boundary condition chosen is that of uniform heat flux at the inner wall and an adiabatic outer wall. The basic numerical procedure used is the SIMPLE algorithm [Int. J. Heat Mass Transfer 15 (1972) 1787] which uses the finite difference method for solving the momentum and energy equations. The investigations reveal that the Nusselt numbers for air are considerably greater than the corresponding values for fully developed mixed convection values over a significant portion of the annular duct. The numerical results were supplemented with some experimentally obtained data.

1. Introduction

The convective mode of heat transfer is of great importance in many engineering applications. A number of investigations have been carried out to study single phase pure forced convection and pure natural convection in different geometries. However, mixed convection, i.e., combined free and forced convection is the most general single phase heat transfer phenomenon and has received considerable attention in recent years. Such a process occurs when the effect of the buoyancy force in forced convection or the effect of forced flow in free convection becomes significant. In mixed convection flows, the forced convection effects and the free convection effects may be of comparable magnitudes.

Mixed convection processes may be divided into external flows over immersed bodies, free boundary flows, and internal flows. In internal flows, mixed convective flows are quite common and there can be a variety of geometries, such as cylindrical, rectangular and triangular cross-sections. The concentric annular duct is of technical importance, as it is used in numerous heat transfer and fluid flow devices involving two fluids. One fluid flows through the inner tube while the other flows through the annular passage between the two tubes. For example, gas-cooled electrical cables, heat exchangers designed for chemical processes require the consideration of mixed convection in an annular flow. Cooling of nuclear fuel rods is another example where the results for the buoyancy-influenced convection in an annulus are useful.

Although mixed convection in horizontal concentric cylinders has been the subject of many investigations for quite some time, there are still many aspects of heat transfer and fluid flow that need to be investigated and understood. A review of literature reveals that most of the available studies on combined free and forced convection heat transfer in horizontal annuli are limited to the fully developed situation [1–8]. Very few studies [9–11] are available on entrance region effect.

The present study deals with a numerical as well as an experimental investigation of steady laminar mixed convection heat transfer in horizontal concentric annuli.

* Corresponding author. Tel.: +91-22-576-7516; fax: +91-22-572-6875.

E-mail address: gks@me.iitb.ernet.in (G.K. Sharma).

0017-9310/01/$ - see front matter
PII: S0017-9310(00)00223-4

Nomenclature

C_p	specific heat, J/kg K
D	diameter, m
D_h	hydraulic diameter, $(D_o - D_i)$, m
g	acceleration due to gravity, m/s^2
Gr	Grashoff number, $(g\beta D_h^4 q)/(v^2 K)$
h	heat transfer coefficient, $q/(T_w - T_b)$, W/ m^2 K
k	thermal conductivity, W/m K
Nu	Nusselt number, hD_h/k
Nu_z	circumferentially averaged Nusselt number
Pr	Prandtl number, $\mu C_p/k$
q	heat flux, W/m^2
r	radial coordinate, radius, m
R	radius ratio, r_o/r_i
Ra	Rayleigh number, $Gr\ Pr$
Re	Reynolds number VD_h/v
T	temperature, °C
T^*	dimensionless temperature, $((T_f - T_{fi})k)/(qD_h)$
V	velocity, m/s
V^*	dimensionless velocity, $V/\bar{V}_z$
$\bar{V}_z$	mean axial velocity, m/s
z	axial coordinate, m
Z_t	dimensionless axial coordinate (thermal), $z/(Re\ Pr\ D_h)$

Greek symbols

β	coefficient of thermal expansion, 1/k
Δ	difference
μ	dynamic viscosity, N s/m^2
v	kinematic viscosity, m^2/s
ρ	density, kg/m^3
θ	tangential coordinate

Subscripts/superscripts

$*$	guessed value or dimensionless value of an entity
f	fluid
h	hydraulic
i	inner, inlet
m	mean
o	outer
r	radial component
w	wall
z	axial component
θ	tangential component

Special attention has been paid to the entrance region effect. The simultaneous development of the velocity and temperature fields is considered by employing the conservation equations of mass, momentum and energy. Various combinations of thermal boundary conditions can be imposed on the surfaces of an annular duct. The combination selected in this study is that of uniform heat flux at the inner wall and an adiabatic outer wall. The numerical method adopted in this work involves the solution of the non-linear, coupled momentum and energy equations. Water is used as the working medium in the experimental investigations.

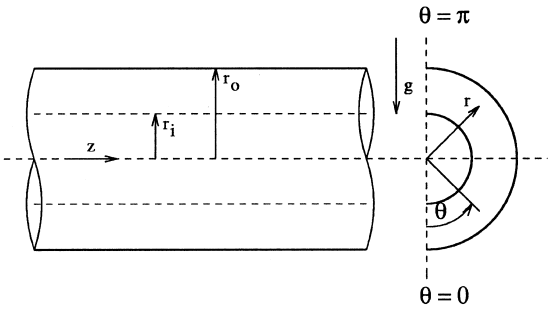

Fig. 1. Coordinate system.

2. Analysis

In view of the annular geometry of the problem a cylindrical coordinate system, as shown in Fig. 1, is selected. The flow is assumed to be symmetric across the vertical plane passing through the axis of the annulus so that calculations need to be done in one vertical half of the geometry only.

The problem is analysed for constant fluid properties with negligible viscous dissipation. The variation of density is taken into account only in the body forces (Boussinesq approximation). The flow is assumed to be a three-dimensional with z-direction as the direction of flow. All terms containing the second derivative of any quantity with respect to z are neglected. It is assumed that

$$V_\theta \ll V_z \quad \text{and} \quad V_r \ll V_z,$$

$$\frac{\partial p}{\partial \theta} \ll \frac{\partial p}{\partial z} \quad \text{and} \quad \frac{\partial p}{\partial r} \ll \frac{\partial p}{\partial z}.$$

The pressure term p is rewritten as

$$p = \bar{p}(z) + p_c(r, \theta, z), \tag{1}$$

where, $\bar{p}(z)$ is an average pressure at z which is a function only of z, and p_c is the deviation from average pressure which is a function of r, θ and z. Since the major flow is in the axial direction, the axial derivative of p_c is neglected in comparison to $d\bar{p}_z/dz$.

All governing equations (conservation of mass, momentum and energy) are expressed in terms of a single general differential equation by combining the convec-

tive and diffusive terms together and presented in the following form with a general dependent variable ϕ:

$$\frac{1}{r}\frac{\partial}{\partial r}\left[(\rho V_r r)\phi - \Gamma r\frac{\partial \phi}{\partial r}\right] + \frac{1}{r}\frac{\partial}{\partial \theta}\left[\rho V_\theta \phi - \frac{\Gamma}{r}\frac{\partial \phi}{\partial \theta}\right] + \frac{\partial}{\partial z}[\rho V_z \phi] = S, \quad (2)$$

where ϕ, Γ and S are as given in Table 1. The following boundary conditions are imposed while solving the governing equations:

1. Symmetry lines ($r_i < r < r_o$; $\theta = 0$ or π):

$$V_\theta = 0, \quad \frac{\partial V_r}{\partial \theta} = 0 \quad \text{and} \quad \frac{\partial T}{\partial \theta} = 0.$$

2. Inner cylinder ($r = r_i$; $0 < \theta < \pi$):

$$V_r = V_\theta = V_z = 0 \quad \text{and} \quad -k\frac{\partial T}{\partial r} = q.$$

3. Outer cylinder ($r = r_o$; $0 < \theta < \pi$):

$$V_r = V_\theta = V_z = 0 \quad \text{and} \quad \frac{\partial T}{\partial r} = 0.$$

4. Inlet ($z = 0$):

$$V_r = V_\theta = 0, \quad V_z = V_{zi} \quad \text{and} \quad T = T_i.$$

The basic numerical procedure [12] adopted in the present study is the SIMPLE algorithm. A finite difference formulation using the control volume-based method is used. The hybrid scheme, with a three-line approximation of the exact solution curve, has been chosen in the present formulation for simplicity. The three-dimensional discretisation equation for a general variable ϕ, with T and B representing the top and bottom neighbours in the z-direction, can be written as

$$a_P\phi_P = a_E\phi_E + a_W\phi_W + a_N\phi_N + a_S\phi_S + a_T\phi_T + a_B\phi_B + b. \quad (3)$$

The equations for conservation of momentum and energy, and the continuity equation can be discretised by taking the respective control volume for each one with the help of Eq. (3). After discretisation, a sequence of steps is followed for solving the equations simultaneously. The procedure involves making a guess of the pressure field and solving the z-direction momentum equation to get the axial velocity. Using the axial velocity, these equations and the energy equation are solved. With the help of the continuity equation, mass balance is checked. If the continuity equation is not satisfied, then a correction to the guessed pressure field is obtained by solving a pressure correction equation. The process is repeated till a satisfactory balance of all equations is achieved. The details of this method are available in [13].

The present numerical code has been benchmarked with the numerical results (Nusselt number, axial velocity profile and mean apparent friction factor) for the case of simultaneously developing laminar flow, pure forced convection heat transfer in an annulus with uniform heat flux at the inner wall and adiabatic outer wall. The numerical code was further tested by comparing the predicted Nusselt numbers with the results of Carlo and Guidice [11] who considered the same problem using finite element method. Fig. 2 shows that the present results are in excellent agreement (±4% with the results of Carlo and Guidice [11].

3. Results and discussion

The numerical investigations were carried out with $10^4 \leqslant Ra \leqslant 10^8$, $1.5 \leqslant R \leqslant 10$, $0.7 \leqslant Pr \leqslant 5.42$ and $200 \leqslant Re \leqslant 1000$. All computations were performed with double precision on a DEC-ALPHA 2100 computer. Although it is intuitive to consider closely packed radial and axial grid spacings near the walls and inlet, respectively, to keep the programme simple, uniform grids were used in all the coordinates. The deviation in Nusselt number with 40×30 and 30×20 grids in the r–θ plane was found to be less than 1% and this deviation reduced (less than 0.5%) with finer grid size (50×50). Grid sensitivity for isotherms and axial, radial and tangential isovels were also on the same lines. Based on this sensitivity results analysis to reduce computer time, a uniform 30×20 grid in the r–θ plane and $\Delta z = 0.25$ mm (leading to $\Delta z/D_h$ ranging from 1/80 to 1/640) has been used in all computations.

3.1. Development of secondary flow

The development of isotherms for $Ra = 10^6$, $Pr = 0.7$, $R = 2$ and $Re = 200$ is shown in Fig. 3. Near

Table 1
Expressions for ϕ, Γ and S

Governing equations	ϕ	Γ	S
Continuity	1	0	0
r-momentum	V_r	μ	$-\frac{\partial p_c}{\partial r} + \rho g\beta(T - T_i)\cos\theta + \frac{\rho V_\theta^2}{r} - \frac{2\mu}{r^2}\frac{\partial V_\theta}{\partial \theta} - \frac{\mu V_\theta}{r^2}$
θ-momentum	V_θ	μ	$-\frac{1}{r}\frac{\partial p_c}{\partial \theta} - \rho g\beta(T - T_i)\sin\theta - \frac{\rho V_r V_\theta}{r} - \frac{2\mu}{r^2}\frac{\partial V_r}{\partial \theta} - \frac{\mu V_\theta}{r^2}$
z-momentum	V_z	μ	$-\frac{\partial p}{\partial z}$
Energy	C_pT	k	0

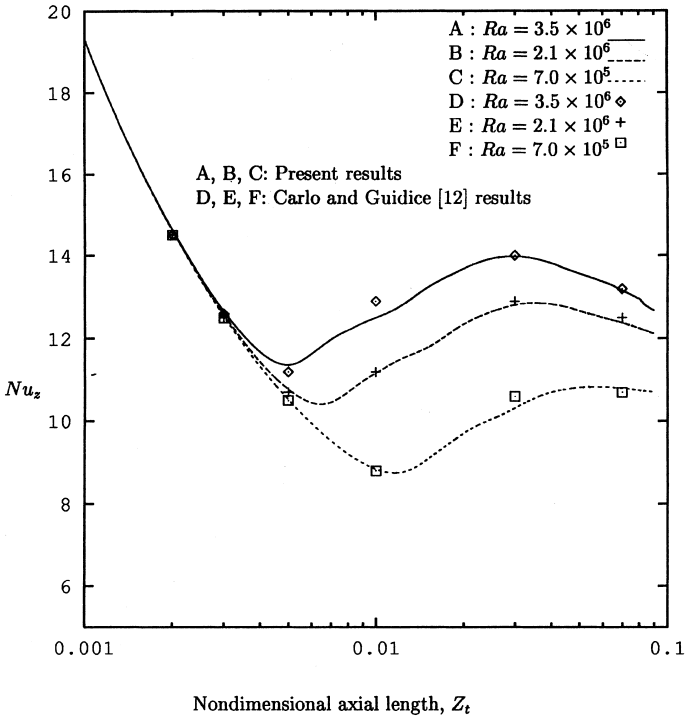

Fig. 2. Comparison of the present results (Nusselt numbers) with the results of Carlo and Guidice [11] for $Pr = 0.7$, $R = 2$ and $Re = 1000$.

the entrance, at $Z_t = 4.46 \times 10^{-3}$ (Fig. 3(a)) the isotherms are almost circular and are virtually unaffected by the secondary flow. At this location, most of the fluid is still at the inlet temperature, and there is little non-uniformity in the temperature distribution. As the fluid moves from the entrance, the buoyancy forces become stronger and start affecting the temperature field. At $Z_t = 1.79 \times 10^{-2}$ (Fig. 3(d)), it is observed that the isotherms at the lower part of the cross-section are still nearly circular, indicating weak secondary motion in this region. The stronger buoyancy effect in the upper half of the cross-section, however, causes noticeable distortion in the temperature field. The isotherms at this location have a tendency to become horizontal, approximating the temperature distribution to that of a stable stratified field. Farther downstream, more thermal stratification takes place, and consequently, the buoyancy forces become stable.

The development of secondary flow due to buoyancy effect is presented in Fig. 4. In order to study the effect of temperature field on the secondary flow pattern, Fig. 4 is plotted for the same values of parameters as for the isotherms in Fig. 3. In the absence of free convection, the radial components of velocities are directed away from the walls of the annulus and the tangential components of velocities are zero. As the free convection effect is included, the secondary flow pattern changes. At $Z_t = 4.46 \times 10^{-3}$ (Fig. 4(a)), a location near the inlet, the magnitude of the secondary velocities is small due to weak buoyancy effect, as is clear from the isotherms in Fig. 3(a). As the fluid proceeds downstream, the strength of the buoyancy forces increases and consequently, the magnitude of the secondary velocities increases. Fig. 4(b), which corresponds to $Z_t = 1.79 \times 10^{-2}$, shows that the secondary velocities in the upper region of the cross-section are of relatively higher magnitude than those in the bottom region. The isotherms (Fig. 3(d)) corresponding to this location, clearly indicate that the buoyancy effect in the upper region of the cross-section is more intense than that in the lower region. It is also noticeable that the fluid near the inner wall rises with relatively high velocity and falls slowly over the rest of cross-section. Since the inner wall is heated, the buoyancy effect causes the fluid near the wall to move upward. It is evident from the nearly circular shape of the isotherms at the bottom region of the cross-section in Fig. 3(d) that the buoyancy effect in this region is still small. Farther downstream (Fig. 4(c) and (d)), the secondary flow becomes weaker, but the qualitative behaviour remains unchanged. Results were obtained for locations at far downstream, where the secondary flow becomes almost stable and the flow is nearly fully developed.

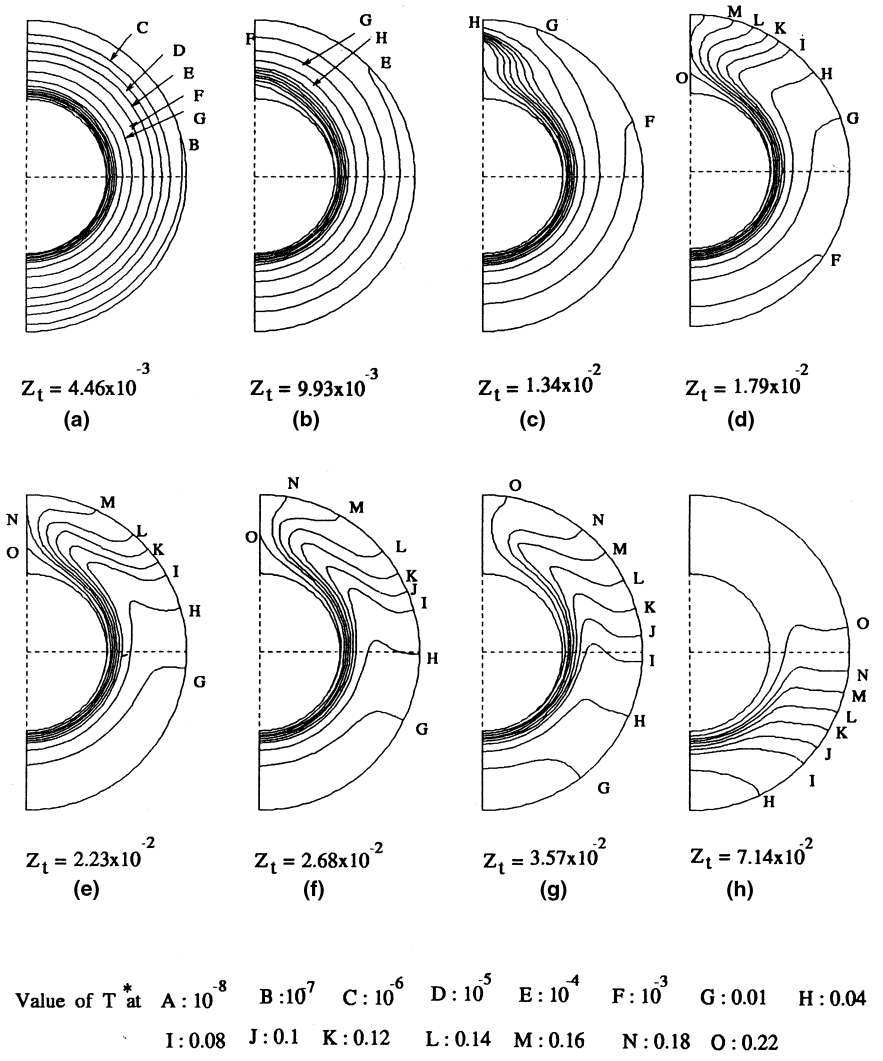

Fig. 3. Development of isotherms for $Ra = 10^6$, $Pr = 0.7$, $R = 2$ and $Re = 200$.

3.2. Development of axial flow

The axial velocity profiles for mixed convection are presented in Fig. 5 with the help of dimensionless axial isovels (V_z^*). In the absence of buoyancy effects, the axial isovels are circular in shape. It is seen in Fig. 5 that the buoyancy-induced secondary flow has a tendency to distort the axial velocity profiles. At $Z_t = 4.46 \times 10^{-3}$ (Fig. 5(a)), a location near the entrance, the axial isovels are seen to be very much similar to those for pure forced convection. This is due to a weak buoyancy effect at this location. As the fluid moves away from the inlet, the axial isovels start deviating from the corresponding axial isovels for pure forced convection. It is seen in Fig. 5(b) that the axial velocities in the top region of the cross-section are highly distorted due to the strong buoyancy effect in this region, whereas little distortion is noticed in the bottom region. This results in nonuniform distribution of axial mass flux, the minimum being at the top and the maximum at the bottom. Farther downstream, the isovels have a tendency for attaining the fully developed situation.

3.3. Effect of Ra on secondary flow

The effect of Rayleigh number on secondary flow has been studied by comparing isotherms, cross-sectional flow patterns and V_z^* isovels at $Z_t = 1.79 \times 10^{-2}$, for $Pr = 0.7$, $R = 2$, $Re = 200$ and for various values of Ra. Fig. 6 shows the effect of Rayleigh number on the isotherms. For $Ra = 10^5$ (Fig. 6(a)), the isotherms are nearly circular in shape. As the Rayleigh number is

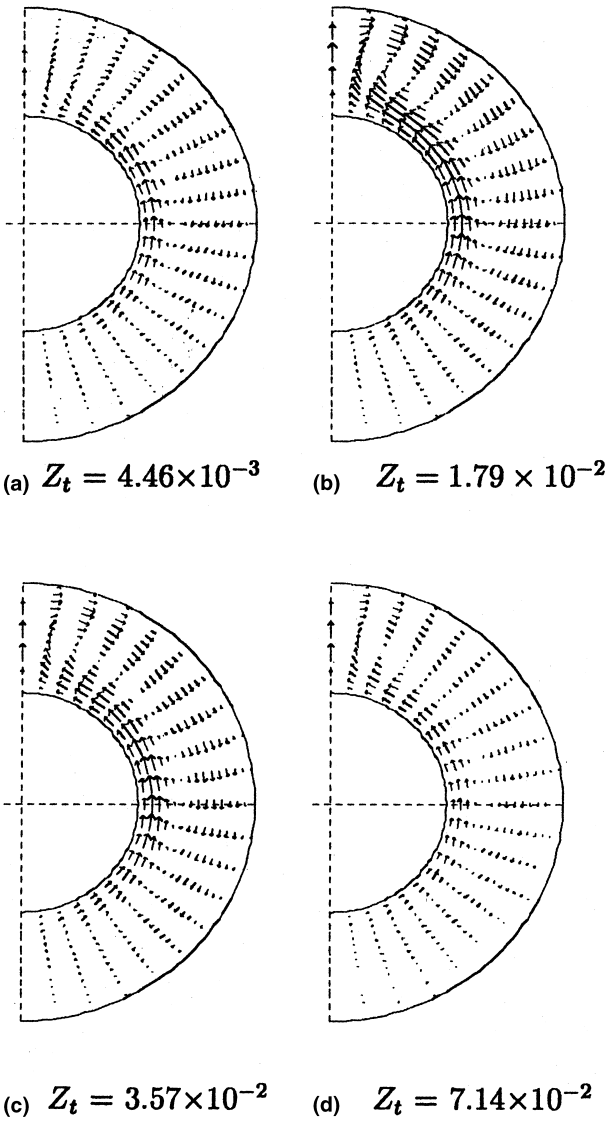

Fig. 4. Development of secondary flow pattern for $Pr = 0.7$, $R = 2$, $Re = 200$, and $Ra = 10^6$.

increased, the isotherms are seen to get more and more distorted, indicating a stronger buoyancy effect. It is noticed that as Rayleigh number increases, the boundary layer on the inner cylinder becomes thinner and the isotherms have a tendency to become horizontal.

The secondary flow pattern is also affected by increasing Rayleigh number. It is observed in Fig. 7(a) that at $Ra = 10^5$, the magnitude of the secondary velocities is very small. As the Rayleigh number increases, the magnitude of the secondary velocities increases. It is important to note that with increasing Rayleigh number, the secondary velocities near the inner wall are greatly affected, whereas the velocities near the outer wall remain essentially unaffected. This is due to the fact that the heat supplied at the inner surface also increases with increasing Rayleigh number and hence, stronger buoyancy effects exist near the inner wall.

3.4. Influence of Ra on axial velocity profile

The effect of Rayleigh number on axial velocity profiles is presented in Fig. 8 for the same values of parameters for isotherms in Fig. 6. As the Rayleigh number increases, the location of maximum velocity at $\theta = 0$ and $\theta = \pi/2$ is seen to be brought nearer to the inner wall, while at the top region ($\theta = \pi$) of the cross-section, with increasing Rayleigh number, the peak has a tendency to shift toward the outer wall. Since the secondary flow at the top region intensifies with increasing Rayleigh number, the distortion in the axial

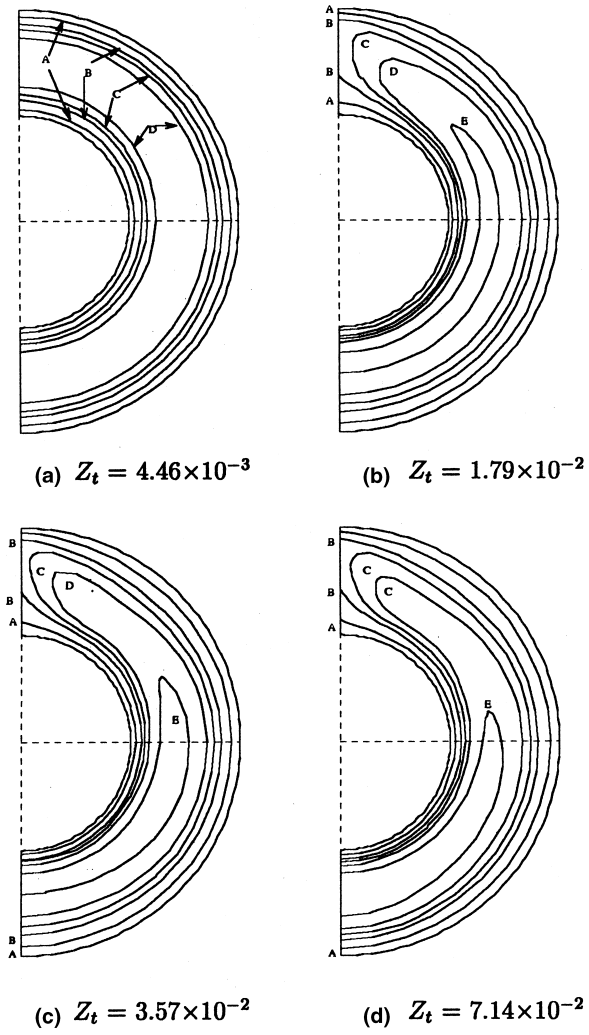

Fig. 5. Development of axial isovels (V_z^*) for $Pr = 0.7$, $R = 2$, $Re = 200$, and $Ra = 10^6$.

velocity profile at this region also increases. It is interesting to note that as the Rayleigh number increases, the discrepancy between the mass fluxes at the top and bottom region of the cross-section increases, the maximum flow being at the bottom and the minimum at the top.

3.5. Heat transfer

The phenomenon of heat transfer has been characterised in terms of circumferentially averaged Nusselt numbers calculated at the inner wall of the annulus where a uniform heat flux is provided. The circumferentially averaged Nusselt number, is obtained as

$$Nu_z = \frac{qD_h}{k(\bar{T}_{wz} - T_b)}, \tag{4}$$

where, $\bar{T}_w$ is the average inner wall temperature and T_b is the bulk fluid temperature at any cross-section. T_b is calculated from

$$T_b = \frac{\int V_z T r \, dr \, d\theta}{\int V_z r \, dr \, d\theta}, \tag{5}$$

where the integrals are evaluated over the cross-section of the annular duct.

Effect of Ra on Nusselt number is presented in Fig. 9. It is seen in Fig. 9 that near the inlet, since the free convection effect is insignificant, all the curves follow the

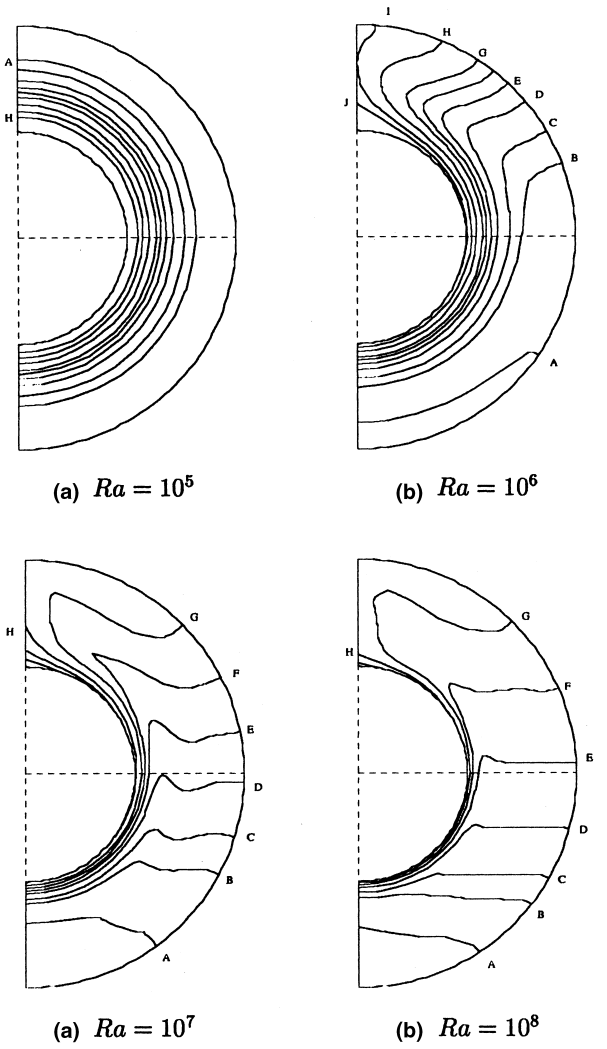

Fig. 6. Influence of Rayleigh number on isotherms (T^*) for $Pr = 0.7$, $R = 2$ and $Re = 200$ at $Z_t = 1.79 \times 10^{-2}$.

pure forced convection ($Ra = 0$) curve. As the buoyancy forces become significant, the curves for combined free and forced convection rise above the pure forced convection curve. At $Ra = 10^5$, the increase in Nusselt number is very modest but becomes appreciable at higher Rayleigh numbers owing to the stronger buoyancy effect. Also with increasing Rayleigh number, the location of maximum Nusselt number shifts toward the inlet. It should be noted that this location roughly corresponds to the axial position where the secondary flow is most vigorous.

After attaining a maximum, the Nusselt number gradually decreases and then attains a practically constant value corresponding to fully developed mixed convection condition. It is observed that, depending on the value of Rayleigh number, the Nusselt numbers are considerably higher than the corresponding pure forced convection values over a significant portion of the annular duct. It can be noted that for $Ra = 10^7$, the Nusselt numbers in the entrance region are 80–150% greater than the corresponding pure forced convection values.

Influence of radius ratio on Nusselt number for $Pr = 0.7$, $Re = 200$ and $Ra = 10^6$ is presented in Fig. 10. The radius ratio curves show that the effect of higher radius ratio is to shift the location of maximum Nusselt number toward the inlet indicating that the thermal

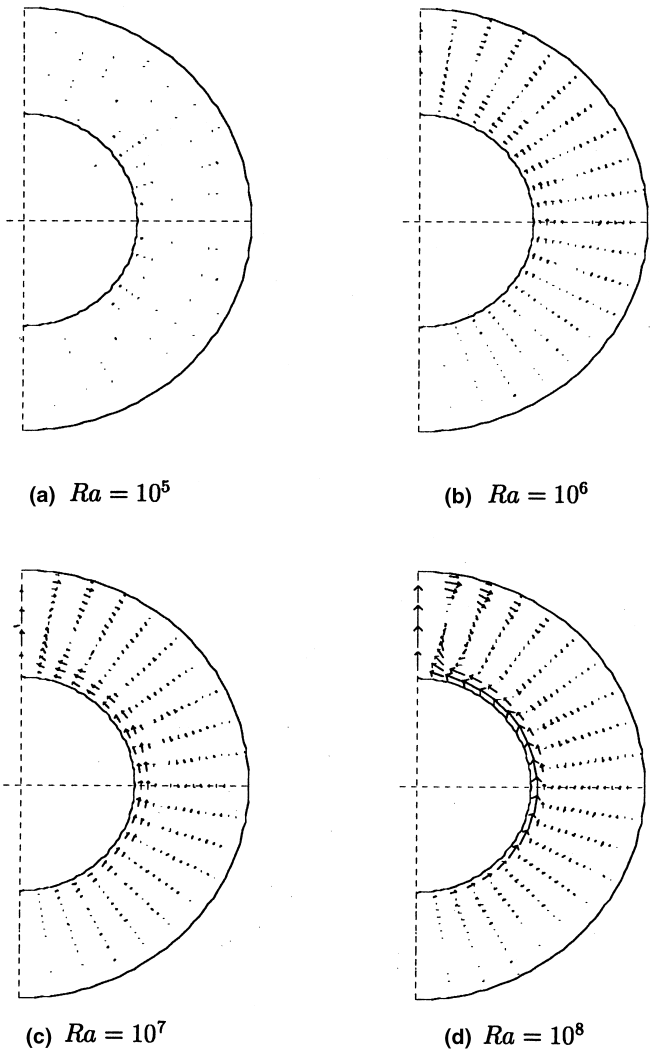

Fig. 7. Influence of Rayleigh number on secondary flow pattern for $Pr = 0.7$, $R = 2$ and $Re = 200$ at $Z_t = 1.79 \times 10^{-2}$.

entrance length (in terms of z/D_h) for higher radius ratio is relatively smaller. However, it is difficult to identifiy an entrance length in these cases because the Nusselt number goes through a minimum, then a maximum, and finally approaches a constant value.

Results concerning the effect of Prandtl number and Reynolds number showed that these parameters had little effect on Nusselt number. It can be mentioned that Z_t is a function of Pr and Re. Hence, it is the consequence of nondimensionalisation of z-axis that Prandtl number and Reynolds number show no significant effect.

3.6. Pressure drop

In the entrance region of an annular duct, apart from the shear pressure drop, part of the pressure drop is attributable to the increase in the total fluid momentum flux, which is associated with the development of the velocity profile. Pressure drop calculation in this region must consider the variation in momentum flux as well as the effects of surface shear forces. The combined effect of surface shear and momentum flux have been incorporated in a single apparent mean friction factor, $\bar{f}_{app}$. The pressure drop from inlet ($z = 0$) to the point of interest (z) is then evaluated from

$$\Delta p = 4\bar{f}_{app}\frac{\rho\bar{V}^2}{2}\frac{z}{D_h}. \tag{6}$$

The pressure drop results are presented with the help of mean apparent friction factor, $\bar{f}_{app}$, plotted against the dimensionless axial length, Z_t. In order to have a realistic assessment of pressure drop characteristics, these figures are plotted for the same values of parameters as in the case of heat transfer characteristics.

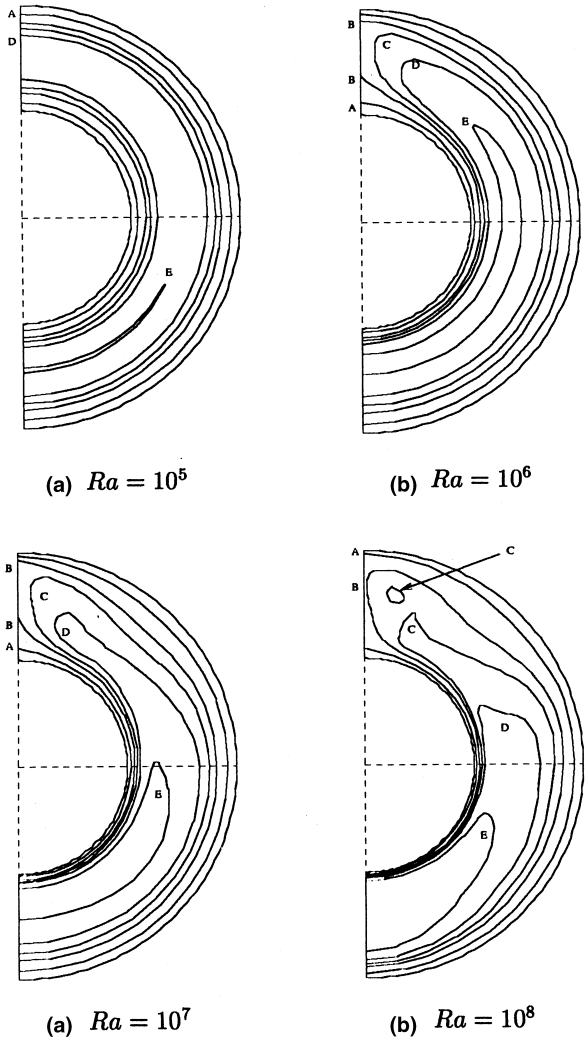

Fig. 8. Influence of Rayleigh number on axial isovels (V_z^*) for $Pr = 0.7$, $R = 2$ and $Re = 200$ at $Z_t = 1.79 \times 10^{-2}$.

The effect of Rayleigh number on mean apparent friction factor is illustrated in Fig. 11. The figure shows that the curve corresponding to $Ra = 10^5$, closely follows the pure forced convection curve, indicating very weak secondary flow. For $Ra > 10^6$, the mean apparent friction factor curves rise above the $Ra = 0$ curve due to higher flow resistance. This indicates that the increased Nusselt number in simultaneously developing mixed convection does not come without a penalty. However, it is important to note that the increase in the value of mean apparent friction factor, $\bar{f}_{app}$, is substantially smaller than the corresponding increase in Nusselt number. For example, the mixed convection Nusselt number for $Ra = 10^7$ and $Z_t = 0.2$ is about 100 % higher than the pure forced convection value at the same location. On the other hand, the corresponding mean apparent friction factor for mixed convection is only about 25% higher than the pure forced convection value.

The effect of Prandtl number on the mean apparent friction factor is shown in Fig. 12 where $\bar{f}_{app}$ is plotted against Z_t. The mean apparent friction factor is seen to be always higher for the lower Prandtl fluid. As the value of Z_t increases, the $\bar{f}_{app}$ for both values of Prandtl numbers tends to become constant, indicating that the flow is approaching the fully developed situation. Results for different radius ratios and Reynolds numbers were also obtained. These results showed that the effect of R and Re on mean apparent friction factor was very small.

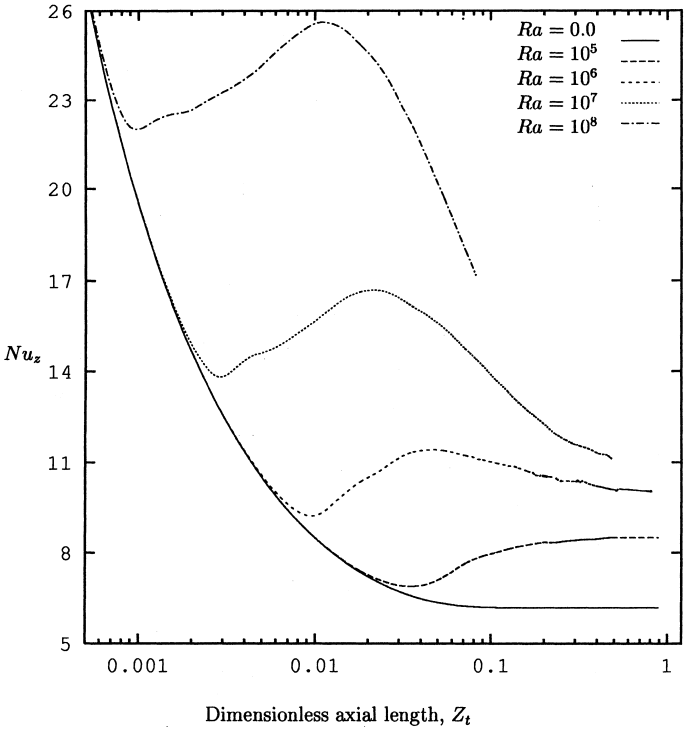

Fig. 9. Influence of Rayleigh number on Nusselt number for $Pr = 0.7$, $R = 2$ and $Re = 200$.

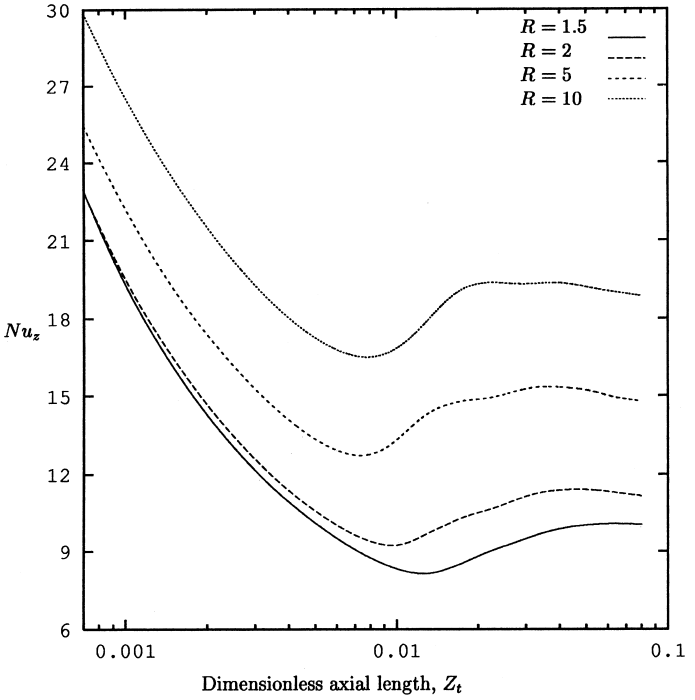

Fig. 10. Influence of radius ratio, R, on Nusselt number Nu for $Pr = 0.7$, $Re = 200$ and $Ra = 10^6$.

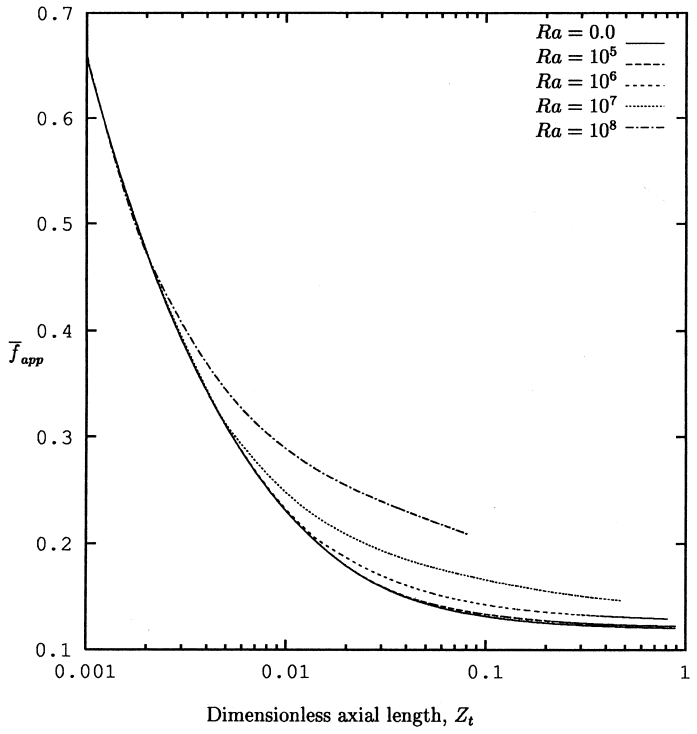

Fig. 11. Influence of Rayleigh number, Ra, on mean apparent friction factor, $\bar{f}_{app}$ for $Pr = 0.7$, $R = 2$ and $Re = 200$.

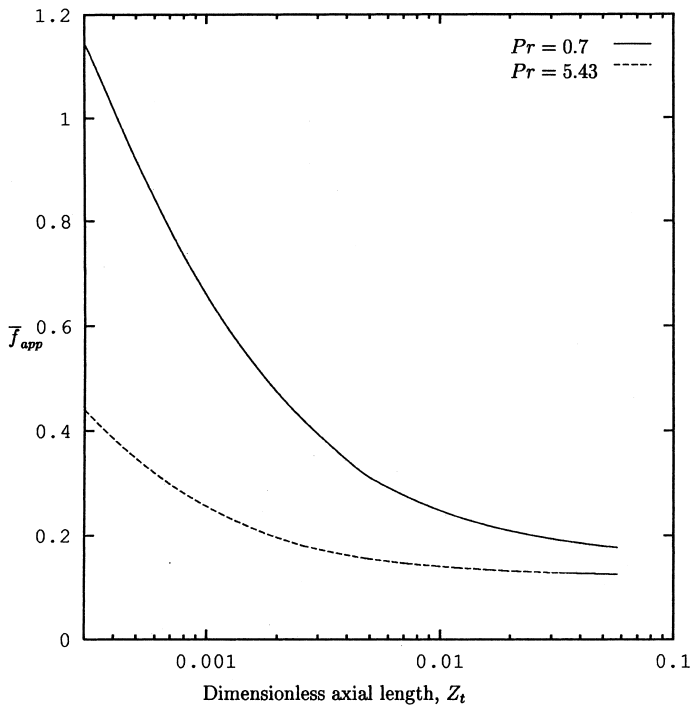

Fig. 12. Influence of Prandtl number, Pr, on mean apparent friction factor, $\bar{f}_{app}$ for $R = 2$, $Re = 200$ and $Ra = 10^7$.

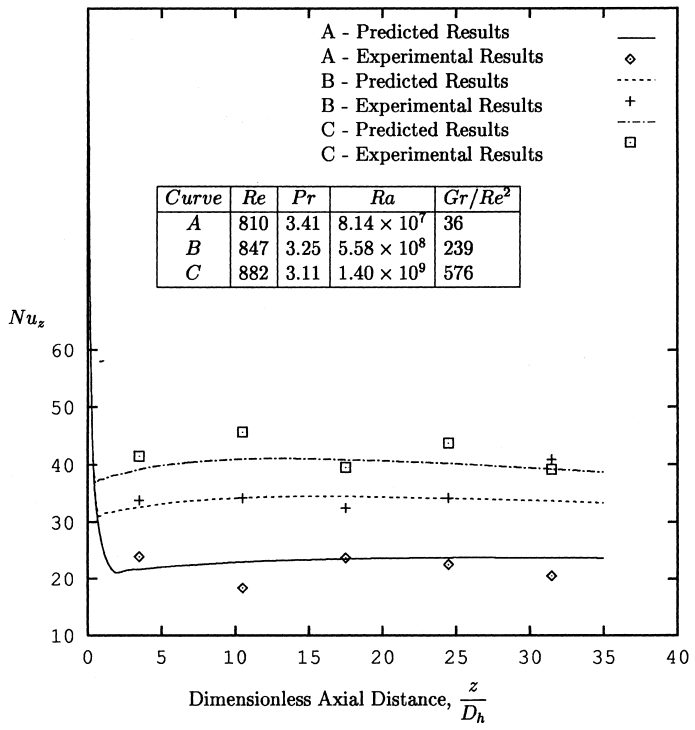

Fig. 13. Comparison of experimental Nusselt numbers with the predicted values for $Pr \simeq 3.25$.

3.7. Comparison of predicted results

The numerical results were supplemented with experimentally obtained data. The details of the experimental investigations are given in [14]. Only necessary results for comparison of predicted and experimental Nusselt numbers are presented here.

The experimental set-up consisted of a test section with a working fluid loop and a cooling water circulating loop. The inner tube of the test section was made of stainless steel and had an effective length of 1.0 m. The outer diameter of the inner tube was 38.1 mm and the wall thickness 1.0 mm. The stainless steel tube was enclosed in a glass tube of 66.7 mm inner diameter to form a horizontal annular passage through which water was made to flow. The test section (inner stainless tube) was provided with 20 copper–constantan thermocouples placed on the outer wall to monitor temperatures at the side, bottom and top positions of the test section at five different axial locations. A honey-comb type flow straightener was placed in the annular space between the copper tube extension and the glass cover to ensure a nearly flat velocity profile at the inlet of the test section. Uniform heat flux at the surface of the test section was provided by passing alternating current through the inner tube of the annulus. A high current three phase to single phase, step down, power transformer capable of supplying 2300 A at 28 V was used for the power supply to the test section.

The comparison of heat transfer results (Nusselt numbers) for $Pr \simeq 3.25$ is presented in Fig. 13. Comparison of Nusselt numbers for different Rayleigh numbers are also presented in Fig. 13. The curves for the numerical results indicate that near the entrance, the Nusselt number decreases rapidly and after a certain axial distance, it gradually increases and then remains uniform. This gradual increase in Nusselt number is so small that it is beyond the scope of the present facility to identify. It is observed in Fig. 13 that the numerical results are in fairly good agreement (±15%) with the experimentally obtained data in the later part of the test section. Although the present experimental investigation was intended to study combined free and forced convection in horizontal annulus with special attention to the entrance region effect, the effective part of the entrance lengths for water is so small that even the first location of measurement does not fall within that range.

4. Conclusions

The numerical code developed has successfully been used to analyse the problem considered. Present results (Nusselt number) were found to agree with the results of

Carlo and Guidice [11] within ±4%. A reasonably good grid sensitivity (±1%) was achieved by using a 30×20 grid in r–θ plane with $\Delta z/D_h$ ranging from 1/640 to 1/80.

The effect of secondary flow due to the buoyancy forces is found to be significant. The secondary flow is more intense in the upper part of the cross-section. It increases throughout the cross-section until its intensity reaches a maximum, and then it becomes weak at far downstream. The development of axial flow and temperature field are strongly influenced by the buoyancy. The buoyancy influence is more pronounced near the inlet section where it is characterised by a deceleration of the axial flow in the upper part of the annulus and an acceleration of the axial flow in the lower part of the annulus. This influence increases with increasing Rayleigh number. At far downstream, however, the interaction between the axial flow and the secondary flow becomes weak.

The effect of increasing the Rayleigh number is to increase both the heat transfer and pressure drop. However, the increase in heat transfer is substantially greater than the corresponding increase in pressure drop. For $Ra = 10^5$ and $Ra = 10^7$, Nusselt numbers at $Z_t = 0.1$ are about 30% and 110% higher than the corresponding pure forced convection Nusselt numbers, respectively. The corresponding increase in mean apparent friction factor due to free convection is only about 4% and 28%, respectively.

The Nusselt number is found to increase with increasing radius ratio. At $Z_t = 0.01$, Nusselt number for $R = 10$ is about 120% higher than that for $R = 1.5$. At $Z_t = 0.8$ also, Nusselt number for $R = 10$ is about 90% higher than that for $R = 1.5$. However, the effect of radius ratio on mean apparent friction factor was found to be insignificant.

The influence of increasing the Prandtl number is to decrease the Nusselt number up to a certain dimensionless axial length, Z_t. After this, Nusselt number increases with increasing Prandtl number. However, the mean friction coefficient decreases with increasing Prandtl number throughout the length. Higher Prandtl number leads to early development of flow. The effect of Reynolds number on Nusselt number as well as mean apparent friction factor is found to be vary small.

The effective part of the entrance lengths for water is so small that it is beyond the scope of the experimental facility to identify. The predicted Nusselt numbers compare well with the experimental results in the later part of the test section where experimental data were obtained. Nusselt number in this region is more or less constant.

References

[1] M. Ciampi, S. Faggiani, W. Grassi, F.P. Incropera, G. Tuoni, Experimental study of mixed convection in horizontal annuli for low Reynolds number, in: Proceedings of the Eighth International Conference on Heat Transfer, vol. 3, 1986, p. 1413.

[2] N. Hattori, S. Kotake, Combined free and forced convection heat transfer for fully developed laminar flow in horizontal tubes (experiments), Trans. JSME 43 (1977) 3379.

[3] N. Hattori, Combined free and forced convection heat transfer for fully developed laminar flow in concentric annuli, numerical analysis, Trans. JSME 45 (1979) 227–239.

[4] A. Mojtabi, J.P. Caltagirone, Analysis du transfer dechaleur en convection mixte laminarie enter deux cylindras coaxial horizentann, Int. J. Heat Mass Transfer 23 (1980) 1369.

[5] T.H. Nguyen, P. Vasseur, L. Robillard, B. Shekhar, Combined free and forced convection of water between horizontal concentric annuli, J. Heat Transfer 105 (1983) 498–500.

[6] S. Kotake, N. Hattori, Combined free and forced convection heat transfer for fully developed laminar flow in concentric annuli, Int. J. Heat Mass Transfer 28 (11) (1985) 2115–2120.

[7] A. Nieckele, S.V. Patankar, Mixed convection in concentric annulus with horizontal axis, J. Heat Transfer 107 (1985) 902–909.

[8] M. Kaviany, Laminar combined convection in a horizontal annulus subject to constant heat flux inner wall and adiabatic outer wall, Trans. ASME, J. Heat Transfer 108 (1986) 392–397.

[9] K.C. Karki, S.V. Patankar, Laminar mixed convection in the entrance region of a horizontal annulus, Numer. Heat Transfer 15 (1989) 87–99.

[10] O. Terhmina, A. Mojtabi, B. Roux, A numerical procedure for three-dimensional mixed convection developing flows in an axisymmetric geometry, Eur. J. Mech., B/Fluids 11 (1) (1992) 21–38.

[11] N. Carlo, S.D. Guidice, Finite element analysis of laminar mixed convection in the entrance region of horizontal annular ducts, Numer. Heat Transfer, Part A 29 (1996) 313–330.

[12] S.V. Patankar, D.B. Spalding, A calculation procedure for heat mass, and momentum transfer in three-dimensional parabolic flows, Int. J. Heat Mass Transfer 15 (1972) 1787.

[13] S.V. Patankar, Numerical Heat Transfer and Fluid Flow, Hemisphere, New York, 1980.

[14] I. Nazrul, U.N. Gaitonde, G.K. Sharma, Combined free and forced convection heat transfer in a horizontal annulus, in: Proceedings of 11th International Conference on Heat Transfer, Kyonjju, Korea, vol. 3, 1998, pp. 299–304.